ELSEVIER

International Journal of Mass Spectrometry 189 (1999) 189–204

International Journal of Mass Spectrometry

Thermochemistry and structures of Na^+ coordinated mono- and disaccharide stereoisomers

Blas A. Cerda, Chrys Wesdemiotis*

Department of Chemistry, The University of Akron, Akron, OH 44325, USA

Received 22 March 1999; accepted 14 April 1999

Abstract

The Na^+ affinities of several mono- and disaccharide stereoisomers are determined in the gas phase based on the dissociations of Na^+-bound heterodimers [saccharide + B_i]Na^+, where B_i represents a reference base of known Na^+ affinity (kinetic method). The compounds investigated include the pentoses arabinose, xylose, and ribose; the hexoses glucose, galactose, and mannose; and the disaccharides melibiose, gentiobiose, and lactose. The decompositions of [saccharide + B_i]Na^+ are assessed as a function of internal energy, to thereby obtain both absolute Na^+ affinities as well as relative entropies of Na^+ attachment. The Na^+ affinities measured are consistent with multidentate coordination of sodium ion by the oxygen sites of the saccharides. In general, hexoses bind Na^+ stronger than pentoses, suggesting that the hydroxymethyl substituent equips them with more conformational flexibility and larger inductive effects for complexing Na^+. The latter properties are further enhanced in the disaccharides, which also carry more basic substituents; as a result, disaccharides form even stronger bonds to Na^+. The entropies of Na^+ attachment are found to rise in the order pentose < hexose < disaccharide, pointing to an increase in this direction of the rotational flexibility lost after attachment of Na^+. The favored [monosaccharide + Na]$^+$ structures predicted computationally contain pyranose rings in chair or boat conformations that permit tri- or tetradentate Na^+ coordination and hydrogen bonds between the hydroxyl ligands; the most stable disaccharide complexes are tetradentate and involve chair forms. In the calculated structures, the pyranose O atom and the hydroxymethyl group(s) generally participate in the Na^+ binding, in agreement with the experimental trends. Small changes in the saccharide stereochemistry alter the optimum Na^+ coordination possible and, therefore, the Na^+ affinity; as a result, the latter thermochemical property is ideally suitable for the distinction of stereoisomeric saccharides. (Int J Mass Spectrom 189 (1999) 189–204) © 1999 Elsevier Science B.V.

Keywords: Na^+ affinity; Na^+ complexes; Saccharides; Entropy effects; Stereoisomer distinction

1. Introduction

The involvement of metal ion–saccharide interactions in key biological processes, such as the binding of metal ions to cell walls [1] and Na^+-glucose transmembrane transport [2], has created immense interest in the gas phase (i.e. intrinsic) chemical properties of the metal ion complexes of saccharides. These properties can readily be explored in the solvent-free environment of the mass spectrometer which, as a result, has enjoyed extensive use in the study of the intrinsic chemistry of metal ion-coordinated sugars. Most mass spectral studies of the Na^+

* Corresponding author. E-mail: wesdemiotis@uakron.edu

PII S1387-3806(99)00085-8

binding to saccharides so far have dealt with the characterization of the fragmentation patterns of [polysaccharide + Na]$^+$ ions, based on which the saccharide's sequence and structure can be deciphered [3–18]. A challenging problem in these efforts is the fact that a given saccharide has a large number of stereoisomers that are difficult to distinguish by conventional (i.e. dissociative) mass and tandem mass spectrometry approaches [19,20]. To overcome this limitation, several investigators have combined novel derivatization and fragmentation techniques, in order to make the differentiation of saccharide stereoisomers a more expedient and/or more accurate process [21–30]. Thermochemistry has recently been recognized as an alternative, sensitive tool for the identification of exact structure and stereochemistry [31–37]. Unfortunately, literature about the thermodynamics of alkali metal ion–saccharide complexes has remained scarce. The knowledge available at this moment is limited to qualitative orders of the alkali metal ion affinities of a few mono- and disaccharides [18,22,38,39]. The present investigation provides first experimental values of the absolute Na^+ affinities of selected pentoses, hexoses, and hexose-based disaccharides and substantiates the usefulness of such data for distinguishing stereoisomers. The affinities are determined by tandem mass spectrometry [19], using the Cooks kinetic method [34,40,41] in a modified version [42,43]. The experimental Na^+ affinities are combined with theoretical calculations to characterize the structures of the [saccharide + Na]$^+$ complexes and rationalize the experimental trends.

2. Thermochemical method

The sodium ion affinity ($\Delta H^o_{Na^+}$) of a saccharide (Sac) corresponds to the dissociation energy of the Sac–Na^+ bond. Cleavage of this bond also causes changes in entropy ($\Delta S^o_{Na^+}$) and free energy ($\Delta G^o_{Na^+}$), which are interrelated via $\Delta G^o_{Na^+} = \Delta H^o_{Na^+} - T\Delta S^o_{Na^+}$. The kinetic method measures relative free energies. Specifically, it compares the rates of dissociation of a Na^+-bound dimer to each of the individual sodiated monomers to estimate the difference in $\Delta G^o_{Na^+}$ between the two monomers. For heterodimers between a saccharide (Sac) and a series of reference bases (B_i), depicted as Sac–Na^+–B_i or [Sac + B_i]Na^+, the pertinent dissociations are

$$\mathrm{Sac} + [B_i]\mathrm{Na}^+ \overset{k_i}{\longleftarrow} [\mathrm{Sac} + B_i]\mathrm{Na}^+ \overset{k}{\longrightarrow} [\mathrm{Sac}]\mathrm{Na}^+ + B_i \quad (1)$$

$$\ln(k/k_i) = \Delta(\Delta G^o_{Na^+})/RT_{eff} = -\Delta(\Delta S^o_{Na^+})/R + \Delta(\Delta H^o_{Na^+})/RT_{eff} \quad (2)$$

The dissociations of Eq. (1) cleave electrostatic bonds, which generally proceeds with no reverse activation energy [44]. In such a case, the natural logarithm of the relative rate constant of the two reactions, i.e. $\ln(k/k_i)$, is given by Eq. (2), where T_{eff} is the effective temperature of the dissociating [Sac + B_i]Na^+ dimer and $\Delta(\Delta G^o_{Na^+})$, $\Delta(\Delta S^o_{Na^+})$, and $\Delta(\Delta H^o_{Na^+})$ are the relative free energy, entropy, and affinity between the Sac–Na^+ and B_i–Na^+ bonds, respectively.

$\Delta(\Delta S^o_{Na^+}) \approx 0$ when the two bases contained in the dimer ion are structurally similar compounds forming the same types of bond(s) to the metal ion bridging them [42,43]. Unfortunately, a set of reference bases (B_i) with *both* known sodium ion affinities *and* saccharide-like structures does not exist. Hence, $\Delta(\Delta S^o_{Na^+}) \neq 0$; nevertheless, this entropy parameter can be kept constant if B_i are chosen to be chemically similar with each other, coordinating Na^+ in an analogous mode; they still may differ from Sac [42,43,45–47]. With this prerequisite, Eq. (2) can be expanded to

$$\ln(k/k_i) = [\Delta H^o_{Na^+}(\mathrm{Sac})/RT_{eff} - \Delta(\Delta S^o_{Na^+})/R] - \Delta H^o_{Na^+}(B_i)/RT_{eff} \quad (3)$$

where the terms remaining constant within a series of heterodimers [Sac + B_i]Na^+ have been combined in brackets. The quantity within brackets represents an apparent free energy of Na^+ attachment to Sac, $\Delta G^{app.}_{Na^+}$(Sac), as defined by Eq. (4).

$$\Delta G^{app}_{Na^+}(Sac)/RT_{eff} = \Delta H^{o}_{Na^+}(Sac)/RT_{eff} - \Delta(\Delta S^{o}_{Na^+})/R \quad (4)$$

$$\Delta(\Delta S^{o}_{Na^+}) = [\Delta G^{app}_{Na^+}(Sac)_{MI} - \Delta G^{app}_{Na^+}(Sac)_{He}]/[T_{He} - T_{MI}] \quad (5)$$

The experiment measures the rate constant ratios k/k_i, which are equal to the ratios of the abundances of $[Sac]Na^+$ and $[B_i]Na^+$ in the tandem mass spectra of $[Sac + B_i]Na^+$. A plot of $\ln(k/k_i)$ versus the known sodium ion affinities of the reference bases, $\Delta H^{o}_{Na^+}(B_i)$, yields T_{eff} and $\Delta G^{app}_{Na^+}(Sac)$. The entropic and enthalpic contributions to $\Delta G^{app}_{Na^+}(Sac)$ can be deconvoluted by determining the rate constant ratios at two or more effective temperatures. T_{eff} is a measure of the internal energy of $[Sac + B_i]Na^+$ [48,49] and can be changed by collisional excitation. Application of Eq. (3) to metastable dimer ions (MI) as well as to dimer ions that have been subjected to collisionally activated dissociation (CAD) with He furnishes two effective temperatures (T_{MI} and T_{He}) and two apparent free energies of Na^+ attachment ($[\Delta G^{app}_{Na^+}]_{MI}$ and $[\Delta G^{app}_{Na^+}]_{He}$) for each saccharide. From this information, $\Delta(\Delta S^{o}_{Na^+})$, i.e. the entropy difference between the Sac–Na^+ and B_i–Na^+ bonds, is calculated according to Eq. (5), and $\Delta H^{o}_{Na^+}(Sac)$, i.e. the sodium ion affinity of the saccharide in question, from Eq. (4) [42]. Alternatively, if more than two T_{eff} values are available, $\Delta(\Delta S^{o}_{Na^+})$ and $\Delta H^{o}_{Na^+}(Sac)$ can be obtained by plotting $\Delta G^{app}_{Na^+}/RT_{eff}$ versus $1/RT_{eff}$ [43,45–47].

The described approach has been used successfully to measure the proton or metal ion affinities of biomolecules, where chemically similar reference bases do not exist [42,43,45–47]. Moreover, the method also assesses relative bond entropies which, combined with the affinity data, can reveal valuable insight about the structure and rotational flexibility of the metalated species and the extent of noncovalent interactions present in them [42,43,45,47].

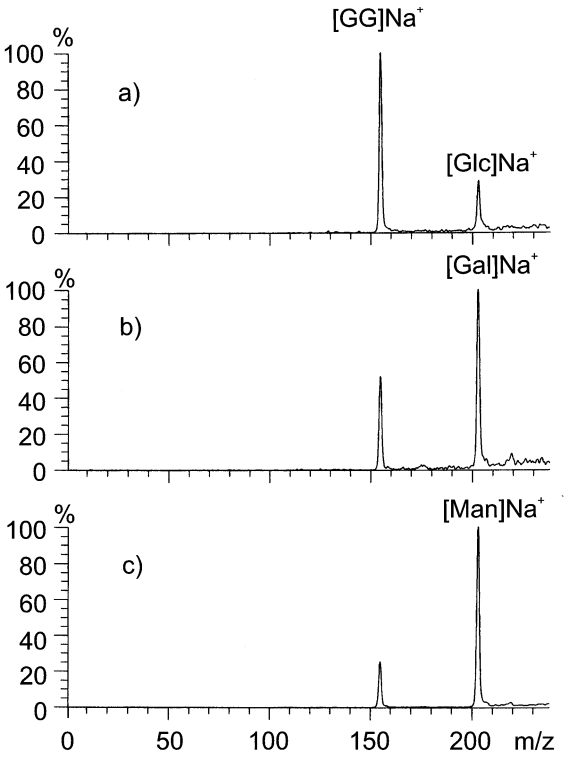

Fig. 1. MI spectra of [hexose + GG]Na^+ ions. (a) Glucose, (b) galactose, and (c) mannose. The $T_{0.5}$ values of the [hexose]Na^+ and [GG]Na^+ peaks in all three spectra are 23 and 18 meV, respectively.

3. Experimental

The experiments were performed with a VG AutoSpec tandem mass spectrometer of E_1BE_2 geometry [50]. Heterodimers $[Sac + B_i]Na^+$ were generated by FAB, using ~12 keV Cs^+ ions as bombarding particles and monothioglycerol as the matrix. The MI and CAD spectra of $[Sac + B_i]Na^+$ were acquired at a kinetic energy of 8 keV as described in detail elsewhere [42,43]. In CAD, the target gas was He or Ar (80% transmittance). The peak widths at half height of all MI signals fall within 23 ± 3 V after correction for the main beam width [51b]. From these peak widths, kinetic energy releases ($T_{0.5}$) were calculated by established procedures [51ab]; representative values are reported in the legends of Figs. 1 and 2. The MI and CAD spectra measured are multiscan summations and reproducible to better than ±5%.

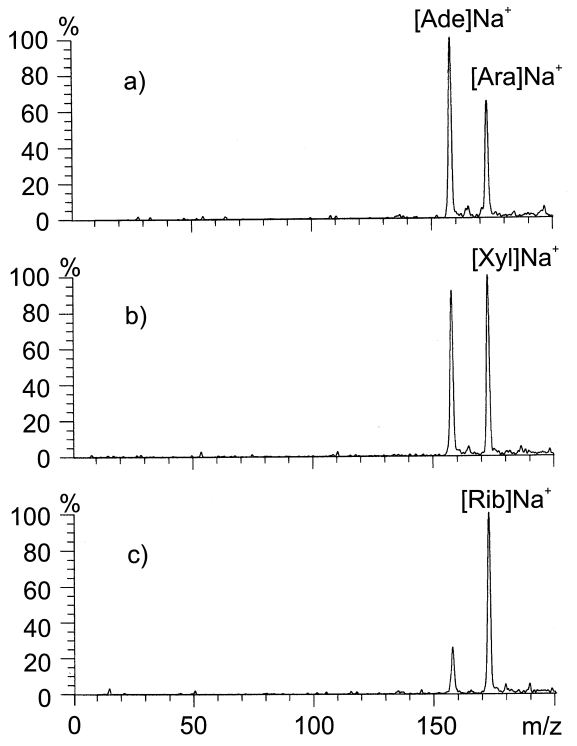

Fig. 2. MI spectra of [pentose + Ade]Na^+ ions. (a) Arabinose, (b) xylose, and (c) ribose. The $T_{0.5}$ values of the [pentose]Na^+ and [Ade]Na^+ peaks in all three spectra are 15 and 13 meV, respectively.

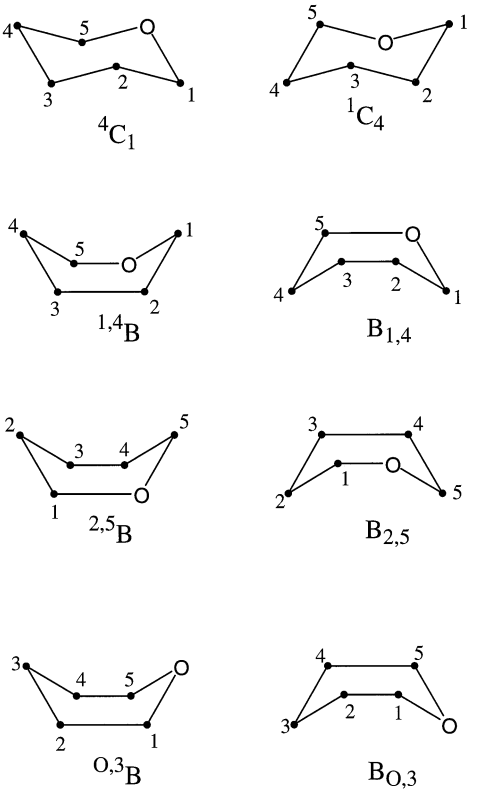

Scheme 1. Pyranose ring conformations considered in the ab initio calculations.

From these spectra, the ratio k/k_i was calculated by dividing the peak heights of [Sac]Na^+ and [B_i]Na^+.

The samples were prepared from saturated solutions in thioglycerol of the appropriate saccharide, reference base, and sodium acetate. To generate the desired heterodimer ion, ~0.5 mL aliquots of the individual stock solutions were mixed and a few microliters of the resulting mixture were transferred onto the FAB probe tip. The pentoses (D-form), hexoses (D-form), and disaccharides as well as sodium acetate and thioglycerol were purchased from Sigma and were used without any modification.

4. Theory

Ab initio calculations were run on a Silicon Graphics O2 station, using Gaussian 94 [52] interfaced with Gaussview [53], or on a pentium PC, using Gaussian 94 for windows interfaced with Chem-3D [54]. Semiempirical calculations and molecular mechanics calculations with the MM2 forcefield were run on the PC using the MOPAC [55] and Chem-3D programs. The structures and energies of the monosaccharide systems were evaluated at the AM1 and several ab initio levels. On the other hand, the geometries of the larger [disaccharide]Na^+ systems were only assessed empirically (MM2).

In solution, the monosaccharides studied exist exclusively or predominantly (≥80%) in the form of cyclic pyranose hemiacetals [56]. Such species can have a large number of distinguishable conformations [56]. For each monosaccharide, the α- and β-anomers of the eight conformers shown in Scheme 1 were considered (16 different conformers per Sac). Na^+ attachment above and below the plane of all 16 Sac

conformers was attempted, resulting in 32 different structures for each [Sac]Na^+ ion. Initial [Sac]Na^+ geometries were obtained by AM1 calculations and reoptimized at the HF/STO-3G level. The Na^+ complexes with at least bidentate coordination, as well as any complex with the ether oxygen and/or the hydroxymethyl group involved as ligands, were subjected to further optimization at the HF/3-21G level. The most stable α- and β-conformers of each [Sac]Na^+ arising in the latter step were optimized at the HF/6-31G* level and the final energies were obtained at the B3LYP/6-311+G(2*d*,2*p*)//HF/6-31G* level. Finally, basis set superposition errors (BSSE) were estimated at the B3LYP/6-311+G(2*d*,2*p*) level with the counterpoise method.

5. Results and discussion

The saccharides studied encompass the pentoses arabinose (Ara), xylose (Xyl), and ribose (Rib); the hexoses glucose (Glc), galactose (Gal), and mannose (Man); and the disaccharides melibiose (Mel), gentiobiose (Gen), and lactose (Lac). Their structures are depicted in Scheme 2, where reducing ends are shown in the pyranose form [56]. The reference bases utilized in the [Sac + B_i]Na^+ dimers were nucleobases (NB) or peptides (Pep). All saccharides studied were compared against the nucleobases guanine (Gua), cytosine (Cyt), and adenine (Ade). Additionally, the monosaccharides were also paired with the dipeptides glycylglycine (GG), glycylalanine (GA), and alanylalanine (AA), in order to corroborate the affinity values and entropy effects deduced with the nucleobase B_i set. The Na^+ affinities of the two B_i sets are summarized in Table 1 [42,43]. Each reference base series consists of chemically similar molecules, coordinating Na^+ in a common fashion (Scheme 3), as required by the kinetic method variant applied here. The Na^+ affinity order determined from [Sac + B_i]Na^+ dimers was further validated by comparing selected saccharides directly to each other in [Sac_1 + Sac_2]Na^+ dimers.

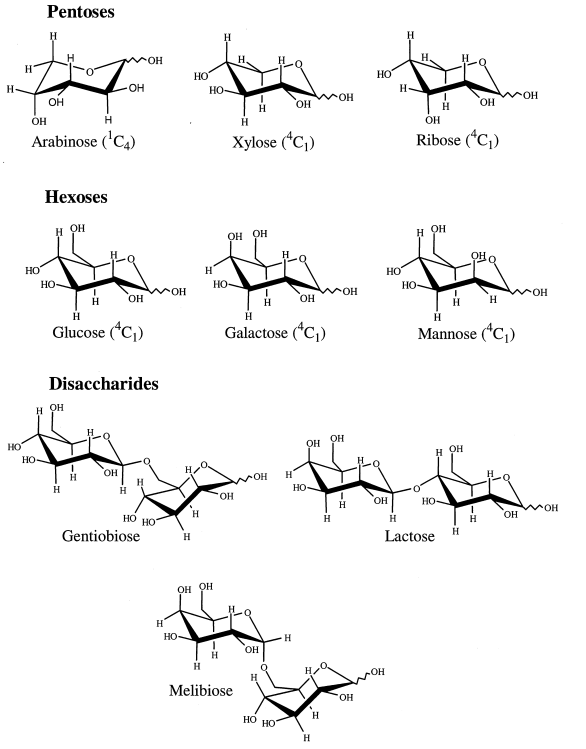

Scheme 2. Pentoses, hexoses, and disaccharides studied. The anomeric C–OH bond in reducing ends (which can be α or β) is depicted by a wavy line. The saccharides are shown in their most stable pyranose conformations [56,59–66].

Table 1
Na^+ affinities of reference bases

Base set (B_i)	$\Delta H^o_{Na^+}(B_i)$[a] (kJ mol^{-1})	Ref.
Nucleobases (NB)		
Adenine (Ade)	172	[42]
Cytosine (Cyt)	177	[42]
Guanine (Gua)	182	[42]
Dipeptides (Pep)		
Glycylglycine (GG)	177	[43]
Glycylalanine (GA)	179	[43]
Alanylalanine (AA)	180	[43]

[a] Determined using the kinetic method and the 298 K Na^+ affinity of N,N-dimethyl formamide as absolute anchor [43]. Hence, the listed $\Delta H^o_{Na^+}(B_i)$ values correspond to 298 K affinities.

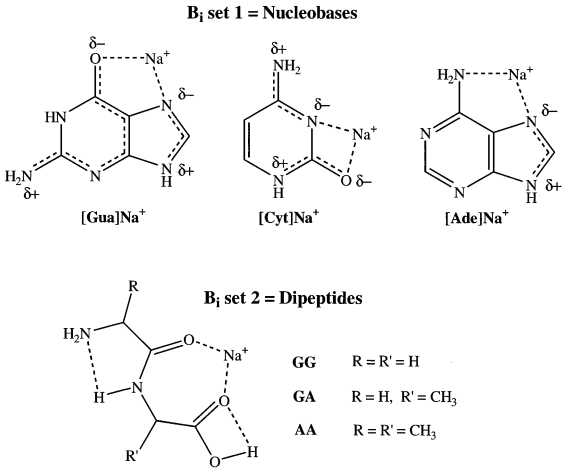

Scheme 3. Structures of [NB]Na^+ (NB = Ade, Cyt, Gua) [42] and [Pep]Na^+ (Pep = GG, GA, AA) [43].

5.1. Tandem mass spectra of the Na^+-bound heterodimers

The MI spectra of dimers [Sac + B_i]Na^+ display essentially two fragment ions, namely [Sac]Na^+ and [B_i]Na^+; this is attested for the isomeric series [hexose + GG]Na^+ and [pentose + Ade]Na^+ in Figs. 1 and 2, respectively. All metastable [Sac]Na^+ and [B_i]Na^+ peaks have Gaussian shape and their peak widths at half height correspond to kinetic energy releases of <25 meV (see legends of Figs. 1 and 2). Such characteristics are consistent with the competitive dissociations of Eq. (1) proceeding without appreciable reverse activation energies [51], as required by the experimental method used.

The competitive eliminations of one Sac or B_i unit remain as the main decomposition channels also after collisional activation, as documented in Fig. 3 by the CAD/He spectrum of [Gal + GA]Na^+. No other significant fragmentation takes place, substantiating that the two bases forming the dimer are weakly bridged via a central Na^+ ion, viz. Sac–Na^+–B_i; this connectivity is a prerequisite for using the kinetic method to determine bond energies (vide supra) [34]. Dimers [Sac_1 + Sac_2]Na^+ show completely parallel features in their MI and CAD spectra.

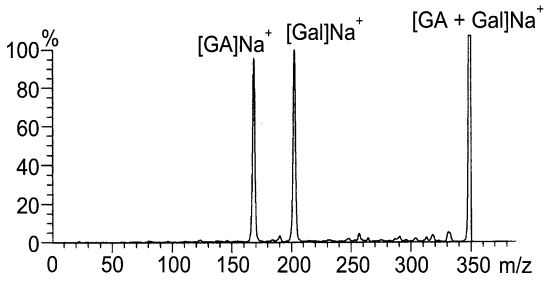

Fig. 3. CAD/He spectrum of [Gal + GA]Na^+.

5.2. From tandem mass spectra to thermochemical data

The dissociations of [Sac + B_i]Na^+ were assessed at two effective temperatures, corresponding to metastable dimer ions (T_{MI}) and to dimer ions that were collisionally activated with He (T_{He}). Figs. 1–3 show relevant MI and CAD spectra, in which the abundance ratio of [Sac]Na^+ to [B_i]Na^+ is equal to the rate constant ratio k/k_i. As exemplified for [Gal + B_i]Na^+ in Fig. 4, plotting $\ln(k/k_i)$ from the MI dissociations versus $\Delta H^o_{Na^+}(B_i)$ affords a regression line whose slope and intercept yield, according to Eq. (3), T_{MI} of [Gal + B_i]Na^+ and the apparent free energy of Na^+ attachment to Gal at T_{MI}, i.e. $\Delta G^{app.}_{Na^+}(Gal)_{MI}$, respectively. Similar treatment of the CAD/He dissociations of [Gal + B_i]Na^+ supplies T_{He} and $\Delta G^{app.}_{Na^+}(Gal)_{He}$ (Fig. 4). This information and Eqs. (4) and (5) allow one to calculate the sodium ion affinity of Gal, i.e. $\Delta H^o_{Na^+}(Gal)$, as well as the relative entropy of the Gal–Na^+ and B_i–Na^+ bonds, i.e. $\Delta(\Delta S^o_{Na^+})$.

Eqs. (4) and (5) presuppose a linear relationship between $\Delta G^{app.}_{Na^+}$ and T_{eff}. To corroborate this presumption, dimers [Rib + Pep]Na^+ and [Lac + NB]Na^+ were also investigated at a third effective temperature, corresponding to CAD with Ar (T_{Ar}). A plot of $\Delta G^{app.}_{Na^+}/RT_{eff}$ versus $1/RT_{eff}$ can then be constructed, as shown for Rib in Fig. 5. The resulting regression line provides $\Delta H^o_{Na^+}$ from the slope and $\Delta(\Delta S^o_{Na^+})$ from the intercept. The so-obtained thermochemical data of Rib and Lac are indistinguishable from those calculated based on only two effective temperatures (Table 2), which is not surprising con-

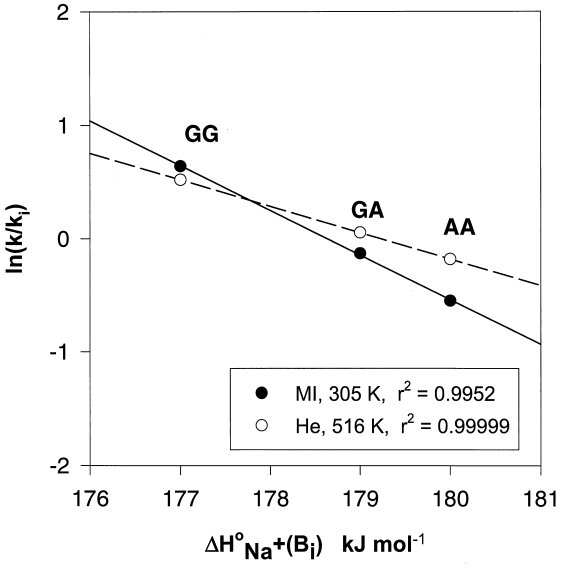

Fig. 4. Plot of $\ln(k/k_i)$ vs. $\Delta H^{o}_{Na^+}(B_i)$ at two effective temperatures for heterodimers [Gal + B_i]Na^+ (B_i = GG, GA, AA). The rate constant ratio k/k_i is equal to the ratio of the abundances of [Gal]Na^+ and [B_i]Na^+ in the corresponding MI (closed circles) and CAD/He (open circles) spectra. The slopes of these lines provide the effective temperatures T_{MI} and T_{He}, while the intercepts provide the apparent free energy of Na^+ attachment to Gal ($\Delta G^{app}_{Na^+}$) at these temperatures, cf. Eq. (3).

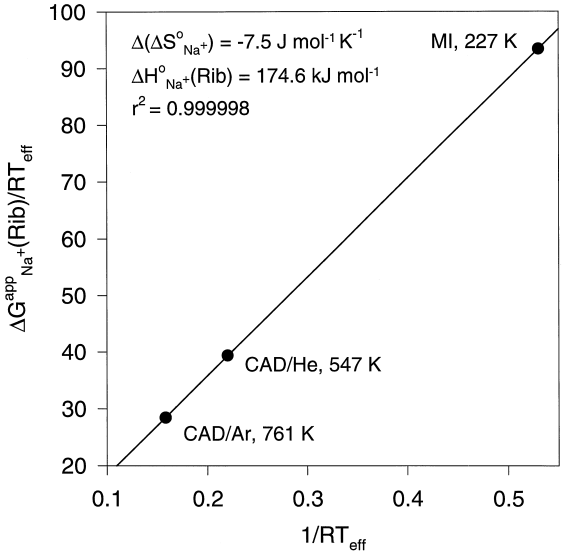

Fig. 5. Plot of $\Delta G^{app}_{Na^+}(Rib)/RT_{eff}$ vs. $1/RT_{eff}$ for heterodimers [Rib + B_i]Na^+ (B_i = GG, AG, AA) and the effective temperatures corresponding to MI, CAD/He, and CAD/Ar spectra. The slope of this line provides the Na^+ affinity of Rib and the intercept provides the relative entropy of the Rib–Na^+ and B_i–Na^+ bonds, cf. Eq. (4).

sidering the excellent linear correlation of Fig. 5. Plots of this type have generally been found to show very high correlation coefficients ($r^2 > 0.999$) [43,45–47], confirming that the apparent free energy of Na^+ attachment depends linearly on effective temperature. Such a result further verifies that $\Delta(\Delta S^{o})$ remains constant for chemically similar reference bases (as assumed) and that it is independent of T_{eff}.

Table 2 summarizes the Na^+ affinities and relative bond entropies deduced for the saccharides studied. The error limits are ± 7 kJ mol^{-1} for $\Delta H^{o}_{Na^+}$ $\pm < 1$ kJ mol^{-1} for $\Delta(\Delta H^{o}_{Na^+})$, and ± 2 J mol^{-1} K^{-1} for $\Delta(\Delta S^{o}_{Na^+})$. The kinetic method can probe very small differences in affinities and, therefore, provides relative thermochemical data with high accuracy [34,37,41–43]; the error limits of absolute values are, however, greater due to the uncertainty in $\Delta H^{o}_{Na^+}(B_i)$.

Replicate measurements of the same [Sac + B_i]Na^+ set lead to effective temperatures lying within $\sim \pm 70$ K for MI and ± 110 K for CAD spectra. T_{eff} of different monosaccharides can vary beyond these experimental reproducibilities (Table 2). The effective temperature reflects the internal energy of the dissociating [Sac + B_i]Na^+ precursor ions [34,48,49] and expectedly increases from MI to CAD conditions (Table 2). T_{MI} and T_{CAD} depend on several factors, including the internal energy distribution upon FAB ionization, the size and structure of the monosaccharide and reference base, the dissociation thresholds of the Sac–Na^+ and B_i–Na^+ bonds in the Sac–Na^+–B_i dimer, and (in CAD) the collisional cross sections of the dimer ions with the target gas used; in addition, T_{eff} is affected by the solubility and concentration of the sample in the FAB matrix [57]. Even under constant experimental conditions, some of this variables cannot be controlled and may cause the observed T_{eff} fluctuations between different saccharide dimers.

5.3. Sodium ion affinities

The Na^+ affinities determined in this study increase in the order Ara < Xyl < Glc < Rib < Gal <

Table 2
Na^+ affinities[a] and relative entropies of Na^+ attachment of the saccharides studied

Saccharide (Sac)	$\Delta G^{app}_{Na^+}(Sac)_{MI}$ (kJ mol^{-1})	T_{MI} (K)	$\Delta G^{app}_{Na^+}(Sac)_{He}$ (kJ mol^{-1})	T_{He} (K)	$\Delta(\Delta S^o_{Na^+})$[b] (J mol^{-1} K^{-1})	$\Delta H^o_{Na^+}(Sac)$[c] (kJ mol^{-1})	Average $\Delta H^o_{Na^+}(Sac)$[d] (kJ mol^{-1})
Monosaccharides							
Arabinose (Ara)							
B_i = NB[e]	171.3	305	169.8	1031	+2.1	171.9	170
B_i = Pep[f]	171.7	401	173.5	614	−8.5	168.3	
Xylose (Xyl)							
B_i = NB[e]	172.9	324	171.4	1286	+1.6	173.4	171
B_i = Pep[f]	172.9	430	175.3	708	−8.6	169.2	
Ribose (Rib)							
B_i = NB[e]	176.1	307	175.8	730	+0.7	176.3	176
B_i = Pep[f,g]	176.2	227	178.9	547	−8.4	174.8	
Glucose (Glc)							
B_i = NB[e]	171.5	436	165.6	1269	+7.1	174.6	174
B_i = Pep[f]	175.9	415	177.5	752	−4.7	174.0	
Galactose (Gal)							
B_i = NB[e]	172.5	476	159.1	2486	+6.7	175.7	177
B_i = Pep[f]	179.0	305	179.5	516	−2.4	178.3	
Mannose (Man)							
B_i = NB[e]	175.0	583	160.8	2149	+8.2	178.5	179
B_i = Pep[f]	179.3	267	180.0	573	−2.3	178.7	
Disaccharides							
Melibiose (Mel)							
B_i = NB[e]	193.3	483	189.9	807	+10.5	198	
Gentiobiose (Gen)							
B_i = NB[e]	195.0	501	190.6	898	+11.1	201	
Lactose (Lac)							
B_i = NB[e,g]	197.6	481	192.2	898	+13.0	204	

[a] Because the reference $\Delta H^o_{Na^+}(B_i)$ data are for 298 K (see footnote a in Table 1), the absolute saccharide affinities derived also are for 298 K.

[b] Calculated by Eq. (5).

[c] Calculated by Eq. (4).

[d] Average value of the affinities resulting from the two base sets used.

[e] NB = nucleobases adenine, cytosine, and guanine.

[f] Pep = dipeptides glycylglycine, glycylalanine, and alanylalanine.

[g] For Rib and Lac, $\Delta G^{app}_{Na^+}$ was also determined using CAD/Ar (T_{Ar}). The corresponding $\Delta G^{app}_{Na^+}/RT_{eff}$ vs. $1/RT_{eff}$ plots (cf. Fig. 5) lead to $\Delta(\Delta S^o_{Na^+}) = -7.5$ J mol^{-1} K^{-1} for Rib vs. Pep and +12.5 J mol^{-1} K^{-1} for Lac vs. NB, and to $\Delta H^o_{Na^+} = 175$ kJ mol^{-1} for Rib and 203 kJ mol^{-1} for Lac.

Man ≪ Mel < Gen < Lac. $\Delta H^o_{Na^+}$ ranges between 170 and 179 kJ mol^{-1} for the monosaccharide and between 198 and 204 for the disaccharide stereoisomers. These values lie considerably above the Na^+ affinities of simpler mono- or bidentate O ligands, such as methanol (111 kJ mol^{-1}) [58], dimethyl ether (93 kJ mol^{-1}) [44], or dimethoxy ethane (161 kJ mol^{-1}) [44], revealing that the saccharides coordinate Na^+ in a multidentate mode (≥2), as expected from their polyfunctional structures and their behavior in solution [56].

The $\Delta H^o_{Na^+}$ order of the monosaccharides is inde-

pendent of the reference base set used (Table 2), pointing out that the same population of [Sac]Na^+ conformers is sampled with either [Sac + NB]Na^+ or [Sac + Pep]Na^+ dimers. The relative affinities between individual monosaccharides, i.e. $\Delta(\Delta H^o_{Na^+})$, vary from 1 to 9 kJ mol^{-1} (Table 2); such values are small but beyond experimental error (<1 kJ mol^{-1}) and larger than the smallest affinity differences measurable by the kinetic method (0.2–0.4 kJ mol^{-1} [34,37]). The ability of the latter method to gauge small changes in Na^+ affinity is clearly evident from the differences observed in the MI spectra of Figs. 1 and 2, which compare isomeric hexoses and pentoses against a dipeptide (GG) or nucleobase (Ade) anchor, respectively. It is noteworthy at this point that the experimental quantity measured (k/k_i) probes directly $\Delta(\Delta H^o_{Na^+})$, not absolute $\Delta H^o_{Na^+}$ values, cf. Eq. (2). Hence, the comparatively larger error limits of absolute affinities (vide supra) do not invalidate the affinity order and relative values derived in this study.

All isomeric mono- or disaccharides exhibit distinguishable Na^+ affinities, demonstrating a correlation between the Sac–Na^+ bond stability and the saccharide's stereochemistry. The reproducibly distinct $\Delta H^o_{Na^+}$ order of epimers, i.e. stereoisomers differing in the configuration at one chiral center (Rib/Ara, Rib/Xyl, Gal/Glc, Glc/Man), further indicates that exact ligand geometry plays an important role in attaining the optimum coordination environment for Na^+. $\Delta H^o_{Na^+}$ increases with the number of O atoms (pentose < hexose ≪ disaccharide), which are potential binding sites [44]. Nevertheless, the lower Na^+ affinity of glucose vis à vis that of ribose shows that a larger number of O sites does not necessarily lead to a higher Na^+–Sac bond energy. Factors, such as the ligand orientation and conformation of Sac and the extent of auxiliary H bonding that can be supported within [Sac]Na^+ need also be considered. The influence of these variables on the stability of [Sac]Na^+ and, hence, $\Delta H^o_{Na^+}$, is examined later by theory.

In protic solvents, reducing saccharides that have the necessary number of carbon atoms exist mainly (≥80%) in the form of cyclic pyranose hemiacetals [56]. For this reason, the thioglycerol solutions subjected to FAB in this study should primarily contain pyranose structures (Scheme 2). Assuming that these pyranoses are desorbed into the gas phase, the affinity data of Table 2 reflect the effects of complexing a sodium ion to pyranose rings with different number and arrangements of hydroxyl substituents. One significant difference between the pyranose ring of pentoses and hexoses is the presence of a hydroxymethyl substituent in the latter (Scheme 2). Such a substituent affords the hexoses a larger conformational flexibility and stronger inductive effects, which would affect their Na^+ binding. Supporting evidence that the hydroxymethyl substituent of the hexoses (and disaccharides) is involved in the complexation of Na^+ comes from the relative entropy data, $\Delta(\Delta S^o_{Na^+})$, listed in Table 2.

5.4. Entropy effects

$\Delta(\Delta S^o_{Na^+})$ represents the difference in entropies between the two bonds compared in the Sac–Na^+–B_i dimer, viz. $\Delta(\Delta S^o_{Na^+}) = \Delta S^o_{Na^+}(Sac) - \Delta S^o_{Na^+}(B_i)$. This parameter depends on the choice of reference bases, as confirmed in Table 2 by the $\Delta(\Delta S^o_{Na^+})$ data of the monosaccharides, which were measured against either NB or Pep molecules as B_i. In previous studies, we have shown that $\Delta(\Delta S^o_{Na^+})$ is related to the structures of the ligands of the Na^+-bound dimer and that it primarily reflects how rotational degrees of freedom in either the biomolecule under study or the reference base are altered upon attachment of the sodium ion [42,43]. The positive $\Delta(\Delta S^o_{Na^+})$ values obtained with [Sac + NB]Na^+ heterodimers indicate that the sugars recover more rotational entropy than the nucleobases once they detach from Na^+. On the other hand, the negative $\Delta(\Delta S^o_{Na^+})$ quantities obtained with [Sac + Pep]Na^+ dimers (Table 2) reveal that Pep recovers more rotational flexibility upon elimination from the dimer than does Sac. It is noteworthy that the relative entropies of [hexose + B_i]Na^+ are more positive (less negative) than those of [pentose + B_i]Na^+ with both B_i sets, strongly suggesting that cleavage of the hexose–Na^+ bond causes a larger entropy gain than cleavage of the pentose–Na^+ bond. This trend can be accounted for if the hydroxymethyl group of the hexoses participates in the coordination

of Na^+. Such an involvement would hinder rotation around the C–CH_2–OH bonds in the metalated species. The restricted rotational degrees of freedom would, however, be recovered (at least partly) when the hexoses are demetalated, thereby giving rise to the mentioned larger entropy gain for the hexoses compared to the pentoses.

The relative entropies of the disaccharides studied (against NB) are even more positive than the relative entropies of the hexoses (against NB). This finding is not surprising, considering that disaccharides possess a larger number of rotors which could be rotationally restricted after Na^+ addition. Interestingly, the largest relative entropy is observed for the disaccharide carrying two hydroxymethyl groups (lactose), presumably because both these groups participate in the binding of Na^+.

5.5. Correlation of the Na^+ affinities to the [Sac]Na^+ structures predicted by theory

Neutral saccharides can exist in a large number of pyranose conformations. The preferred pyranoses contain chairs with most substituents in equatorial positions (Scheme 2), both in solution [56] and the gas phase [59–66]. The best coordination of Na^+ may, however, be achieved by less stable chair or boat conformers that can more efficiently solvate the metal ion. Due to such conformational complexity, it is very difficult to assess the structure of the [Sac]Na^+ complexes from the experimental data alone. To obtain more information on the nature of the Sac–Na^+ bond, the geometries and energies of several [Sac]Na^+ conformers have been interrogated computationally.

5.5.1. Hexoses and pentoses

The monosaccharide conformers considered (Scheme 1) are the α- and β-anomers of the eight basic pyranose rings, which include the $^4C_1$ and $^1C_4$ chair forms and the $^{1,4}B$, $B_{1,4}$, $^{2,5}B$, $B_{2,5}$, $^{0,3}B$, and $B_{0,3}$ boat forms [56]. Other, more strained conformations, such as the skew, half-chair, and sofa forms, which are less common in solution, were not investigated. The customarily used numbering of the C and O atoms in pyranose rings of pentoses and hexoses is given in Scheme 4.

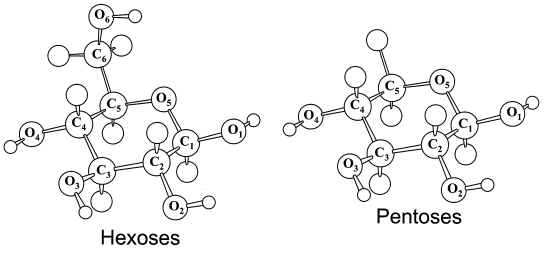

Scheme 4. Numbering of the heavy atoms in the pyranose rings of pentoses and hexoses.

The α- and β-anomers of each monosaccharide were examined in the eight chair and boat conformations mentioned previously. The geometries and energies of the complexes arising by Na^+ attachment above and below the plane of these conformers were calculated at various ab initio levels. Results at the HF/3-21G level of theory indicate that structures with only monodentate coordination of Na^+ are higher in energy than multidentate conformers. For complexes offering the same number of ligands to Na^+, those involving the hemiacetal oxygen of the pyranose ring are found to be lower in energy. Similarly, the hexose conformers with a binding interaction between Na^+ and the hydroxymethyl group are lower in energy than those in which the hydroxymethyl group is only involved in H bonding. It is further observed that several chair conformers of [Sac]Na^+ collapse into boats or sofas upon optimization in order to increase the number of ligands to Na^+. The lower energy [Sac]Na^+ complexes are tri- or tetradentate and contain Na^+ bound to the hemiacetal oxygen and at least two hydroxyl groups of the pentoses, or to the hemiacetal oxygen, the hydroxymethyl group, and at least one additional hydroxyl group of the hexoses. Optimization of the most stable α- and β-anomers of each [Sac]Na^+ at the HF/6-31G* level of theory leads to the geometries shown in Figs. 6 and 7. Table 3 presents the relative energies of these conformers at several levels of theory.

Fig. 6 reveals that β-[Glc]Na^+, β-[Gal]Na^+, and β-[Man]Na^+ are tetradentate complexes with the same type of ligands to Na^+. In the β-[Man]Na^+

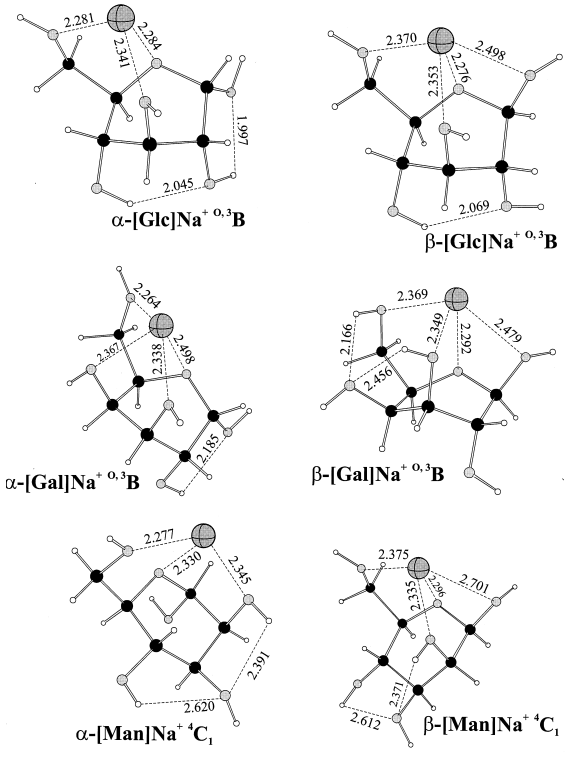

Fig. 6. HF/6-31G* optimized geometries of the most stable α- and β-conformers of [hexose]Na^+. Bonding interactions are indicated by dashed lines and the corresponding bond lengths are given in angstroms.

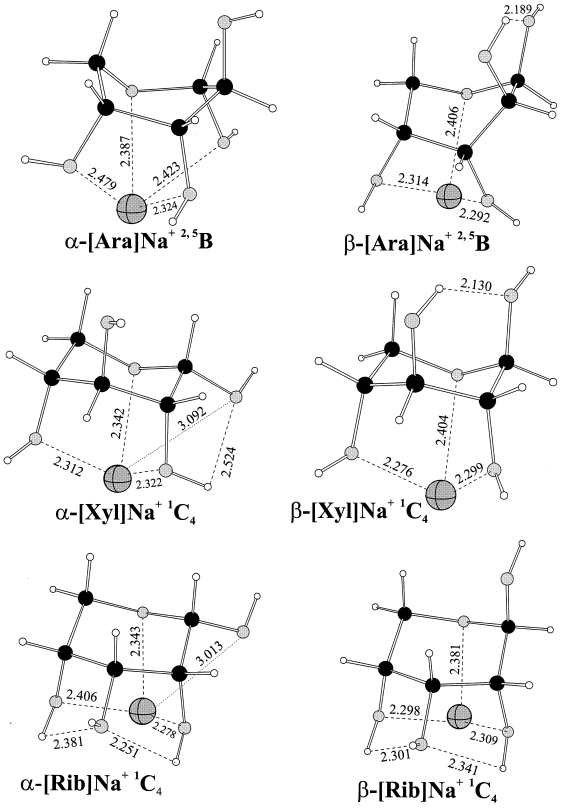

Fig. 7. HF/6-31G* optimized geometries of the most stable α- and β-conformers of [pentose]Na^+. Bonding interactions are indicated by dashed lines and the corresponding bond lengths are given in angstroms.

complex, Na^+ is solvated by the $^4C_1$ chair of mannose; in contrast, Glc and Gal have to adopt the less favorable $^{0,3}B$ boat ring structure in order to provide the most efficient coordination to Na^+, explaining the lower stability of the β-[Glc]Na^+ and β-[Gal]Na^+ systems versus β-[Man]Na^+ (Table 3). β-[Glc]Na^+ and β-[Gal]Na^+ are epimers, differing only in the position of the hydroxyl group at O_4, which is axial in $^{0,3}B$ β-[Glc]Na^+ and equatorial in $^{0,3}B$ β-[Gal]Na^+. The equatorial O_4-hydroxyl group of β-[Gal]Na^+ can form two hydrogen bonds, viz. with the O_6-hydroxymethyl and O_3-hydroxyl substituents (Fig. 6). On the other hand, the axial O_4-hydroxyl group of β-[Glc]Na^+ allows for only one stabilizing hydrogen bond (to O_2), resulting in a lower stability for β-[Glc]Na^+ versus β-[Gal]Na^+ (Table 3). The importance of such small stereochemical differences on the energy of the corresponding structures is reiterated by the Na^+ adducts of epimers β-Glc and β-Man. In their $^4C_1$ chair, these two sugars differ in the position of the O_2-hydroxyl group, which is equatorial in β-Glc and axial in β-Man (Scheme 2). The hydroxyl groups at O_1, O_2, and O_3 are equatorial–axial–equatorial for β-Man and equatorial–equatorial–equatorial for β-Glc. The equatorial–axial–equatorial sequence in β-Man allows the $^4C_1$ chair to coordinate an approaching Na^+ ion in a tetradentate fashion without too much strain on the $^4C_1$ ring (Fig. 6). With the equatorial–equatorial–equatorial sequence of β-Glc such tetradentate coordination is, however, impossible; to achieve this, β-Glc adopts the $^{0,3}B$ boat form in which the O_1-, O_2-, and O_3-hydroxyl groups become equatorial–axial–axial and, thus, capable of supporting tetradentate coordination (Fig. 6). A very

Table 3
Relative energies of the most stable α- and β-anomers of [monosaccharide]Na^+ at different computational levels (kJ mol^{-1}). The [pentose]Na^+ and [hexose]Na^+ complexes are ranked separately, relative to the most stable isomer.

Complex	Pyranose form	HF/3-21G	HF/6-31G*	B3LYP/6-311+G(2*d*,2*p*)//HF/6-31G*	B3LYP/6-311+G(2*d*,2*p*)+ BSSE//HF/6-31G*
Pentoses					
α-[Ara]Na^+	$^{2,5}B$	37.6	39.1	35.5	36.1
β-[Ara]Na^+	$^{2,5}B$	43.5	45.6	41.8	41.7
α-[Xyl]Na^+	$^1C_4$	14.2	7.6	9.6	10.0
β-[Xyl]Na^+	$^1C_4$	21.3	25.6	23.2	23.6
α-[Rib]Na^+	$^1C_4$	15.8	4.5	3.2	4.2
β-[Rib]Na^+	$^1C_4$	0.0	0.0	0.0	0.0
Hexoses					
α-[Glc]Na^+	$^{0,3}B$	38.3	47.3	34.9	34.9
β-[Glc]Na^+	$^{0,3}B$	13.7	28.4	28.1	28.5
α-[Gal]Na^+	$^{0,3}B$	6.9	21.1	22.9	23.8
β-[Gal]Na^+	$^{0,3}B$	0.0	18.4	20.6	21.0
α-[Man]Na^+	$^4C_1$	7.6	5.1	3.0	2.8
β-[Man]Na^+	$^4C_1$	5.0	0.0	0.0	0.0

similar situation pertains to β-Gal, which is a diastereomer of β-Man. The hydroxyl disposition at O_1, O_2, and O_3 in the $^4C_1$ chair of β-Gal is equatorial–equatorial–equatorial (Scheme 2); again, such an arrangement cannot offer tetradentate coordination. If the pyranose conformation is changed from $^4C_1$ to $^{0,3}B$, however, the mentioned hydroxyl groups of β-Gal attain an equatorial–axial–axial sequence that enables tetradentate coordination (Fig. 6). Obviously, the exact stereochemistry of the hexoses plays an important role in determining the conformation of the pyranose rings that will best solvate the Na^+ ion.

The computationally predicted structures for the α-anomers of [hexose]Na^+ contain the same pyranose conformation as the β-anomers but different Na^+ coordination environments (cf. Fig. 6). The most obvious changes occur for α-Glc and α-Man, whose Na^+ complexes are tridentate whereas those of β-Glc and β-Man were tetradentate (vide supra). Both anomers of [Gal]Na^+ are tetradentate but differ in one Na^+ ligand; specifically, the O_1-hydroxyl group in β-[Gal]Na^+ is replaced by the O_4-hydroxyl group in α-[Gal]Na^+ (Fig. 6). Overall, the stability order of the α complexes is α-[Man]Na^+ > α-[Gal]Na^+ > α-[Glc]Na^+. The ranking α-[Gal]Na^+ > α-[Glc]Na^+ reflects the larger coordination number in the $^{0,3}B$ boat of α-[Gal]Na^+; similarly, the ranking α-[Man]Na^+ ($^4C_1$) > α-[Glc]Na^+ ($^{0,3}B$) reflects the higher intrinsic stability of a tridentate chair versus a tridentate boat conformation. Further, the order α-[Man]Na^+ ($^4C_1$) > α-[Gal]Na^+ ($^{0,3}B$) reveals that an intrinsically more stable chair ligand can yield a lower energy complex than a more strained boat ligand with a larger number of binding sites (Fig. 6). Overall, the α-anomers of [hexose]Na^+ are less stable than the respective β-anomers (Table 3).

The conformations adopted by the corresponding most stable [pentose]Na^+ ions are $^{2,5}B$ in [Ara]Na^+ and $^1C_4$ in [Xyl]Na^+ and [Rib]Na^+ (Fig. 7). The $^4C_1$ chair of neutral Xyl has an equatorial–equatorial–equatorial sequence of the O_2-, O_3-, and O_4-hydroxyl groups, the anomeric OH group (O_1) being axial in the α- and equatorial in the β-form (Scheme 2). $^4C_1$ Rib, an epimer of Xyl (Scheme 2), carries an equatorial–axial–equatorial sequence at O_2, O_3, and O_4 and an axial (α) or equatorial (β) anomeric group (O_1). Such stereochemistry does not permit a tridentate Na^+ ligation that would include the ether oxygen. Consequently, these two pentoses adopt the $^1C_4$ chair, in which the sequences for O_2, O_3, and O_4 become axial–axial–axial for Xyl and axial–equatorial–axial for Rib (Fig. 7). Now, the two axial hydroxyl groups placed below the ring plane (O_2 and O_4) and the hemiacetal oxygen (O_5) allow for at least tridentate

interactions. The $^1C_4$ chair of Ara (epimer of Rib and diastereomer of Xyl) contains an equatorial–equatorial–axial sequence of OH groups (O_2, O_3, and O_4) as well as an equatorial (α) or axial (β) hydroxyl group at the anomeric center (Scheme 2). Neither tri- nor tetradentate coordination is possible with such stereochemical dispositions. For the most stable [Ara]Na^+ complexes, a change to the $^{2,5}B$ pyranose structure is necessary, which possesses three axial hydroxyl groups (O_1, O_3, and O_4) below the ring plane in the α- and two (O_3 and O_4) in the β-anomer, thus making it possible to form tetra- and tridentate complexes, respectively, as depicted in Fig. 7.

The higher stability of [Rib]Na^+ and [Xyl]Na^+, as compared to [Ara]Na^+ (Table 3), can be assigned to the intrinsically more favorable chair conformations of the former vs. the less favorable boat structure of the latter. The lower energy of [Rib]Na^+ versus [Xyl]Na^+, which carry similarly coordinated Na^+ ions, is due to the position of O_3. The equatorial hydroxyl group in [Rib]Na^+ can develop two stabilizing hydrogen bonds with the O_2- and O_4-hydroxyl groups (Fig. 7); in contrast, the axial O_3 in [Xyl]Na^+ permits the formation of only one H bond (between O_1/O_3 in the β- and O_1/O_2 in the α-anomer). It is noticed that α-[Ara]Na^+, a tetradentate complex, is higher in energy than tridentate α-[Rib]Na^+ and α-[Xyl]Na^+. Apparently, the stabilizing effects of tetradentate coordination are overcome by the less favorable boat structure adopted by α-[Ara]Na^+. For Ara and Xyl, the α complexes are more stable than the corresponding β complexes; the reverse is true for Rib which parallels the behavior encountered with the hexoses, yielding a more stable β complex.

Overall, the ab initio calculations predict that the monosaccharides will associate with Na^+ in the chair or boat conformation that represents the best compromise between the most favorable ring structure and the highest degree of Na^+ solvation. The structures adopted lead to the stability ranking [Man]Na^+ > [Gal]Na^+ > [Glc]Na^+ for the α- or β-hexoses, and [Rib]Na^+ > [Xyl]Na^+ > [Ara]Na^+ for the α- or β-pentoses (Table 3). It is noteworthy that these orders are common to both anomers of the complexes; they also match the experimentally derived Na^+ affinity scales of the hexoses (Man > Gal > Glc) and pentoses (Rib > Xyl > Ara), cf. Table 2. This qualitative agreement indicates that the Sac–Na^+ bond strengths partially reflect the thermodynamic stability of the Na^+ complexes.

Our experimental data originate from the competitive decompositions of [Sac + B_i]Na^+ dimers. These dimer ions, which may be preformed in the FAB matrix or arise by ion–molecule reactions in the selvedge region, could contain varying proportions of the α- and β-Sac anomers. The anomeric composition of [Sac + B_i]Na^+ would not affect the $\Delta H^o_{Na^+}$ order, because both anomers follow the same stability trends (vide supra). The internal energy distributions of the [Sac + NB]Na^+ and [Sac + Pep]Na^+ dimers studied most likely differ due to the quite different structures of NB versus Pep; still, the same affinity order is obtained with both B_i sets, pointing out that the metastable and collision induced fragmentations from both types of dimers lead to the same [Sac]Na^+ structures. The agreement between the experimental $\Delta H^o_{Na^+}$ order of the pentoses and hexoses (Table 2) and the theoretically predicted order for the lowest energy [pentose]Na^+ and [hexose]Na^+ conformers (Table 3) further suggests that the dissociations Sac–Na^+–B_i → [Sac]Na^+ + B_i yield the most stable [Sac]Na^+ structure. During the competing dissociations Sac–Na^+–B_i → Sac + [B_i]Na^+, most monosaccharides must undergo rearrangement in order to form the most stable neutral Sac chair from the conformation present in the sodiated species; for example, cleavage of the Glc–Na^+ bond in Glc–Na^+–B_i necessitates isomerization of the $^{0,3}B$ boat in Na^+-bound glucose (Fig. 6) to the $^4C_1$ chair of neutral glucose (Scheme 2). The conversions "boat → chair" or "chair → inverted chair" require low activation energies (<50 kJ mol^{-1} in six-membered rings [67]), however, and should be facile at the energies needed to break even monodentate Na^+–ether bonds (>90 kJ mol^{-1} [44]). This expectation is supported by the small kinetic energy releases observed upon [Sac]Na^+ and [B_i]Na^+ formation from the dimers, which are consistent with no reverse barriers for the Sac–Na^+ and B_i–Na^+ bond cleavages (vide supra). Based on these arguments, it is tentatively concluded

that the experimental Na^+ affinities reflect the energy difference between the ground states of sodiated and neutral saccharide.

Although the qualitative experimental and theoretical trends are in consent, it should be mentioned that the affinity differences between individual pentoses or hexoses (Table 2) and the energy differences of the corresponding [pentose]Na^+ and [hexose]Na^+ complexes (Table 3) do not agree quantitatively. This could (in part) be the result of the low level of calculations used, which may be inadequate to locate the true global minima of species with a large number of isomers.

5.5.2. Disaccharides

Because of the large number of heavy atoms in the disaccharides lactose, gentiobiose, and melibiose, their interactions with Na^+ were only examined by molecular mechanics with the MM2 force field. In the conformers considered, both monosaccharide constituents interacted with Na^+. Simultaneous coordination of Na^+ by the hydroxymethyl group(s), the pyranose hemiacetal oxygen, and the glycosidic oxygen were compared against conformations in which the aforementioned ligands were progressively replaced with hydroxyl groups. Fig. 8 presents the lowest energy conformers located for the three disaccharides. A striking common feature is that the glycosidic oxygen does not participate in the binding of Na^+. All three disaccharides offer tetradentate coordination. In lactose, Na^+ is bound to both hydroxymethyl groups as well as to the hemiacetal oxygen and one hydroxyl group of the nonreducing pyranose ring; in gentiobiose and melibiose, Na^+ is bound to the hydroxymethyl group and hemiacetal oxygen of the nonreducing ring, and to the hemiacetal oxygen and anomeric hydroxyl group of the reducing ring. The relative stabilities of the disaccharide complexes increase in the order [Mel]Na^+ < [Gen]Na^+ < [Lac]Na^+ (Fig. 8), which reproduces our experimentally derived Na^+ affinity order melibiose < gentiobiose < lactose (Table 2). The experimental $\Delta H^{\circ}_{Na^+}$ values also reveal that disaccharides bind Na^+ stronger than monosaccharides. The theoretically predicted structures of the corresponding Na^+ complexes provide several reasons for this observation. Based on the structures of [monosaccharide]Na^+ (Figs. 6 and 7) and [disaccharide]Na^+ (Fig. 8), the most stable coordination environment is reached when the binding sites include pyranose oxygens (intrinsically more basic to Na^+ than hydroxyl groups) and hydroxymethyl groups (more flexible in approaching Na^+). Disaccharides contain more of these better ligands. Additionally, the higher Na^+ affinities of the disaccharides are also the

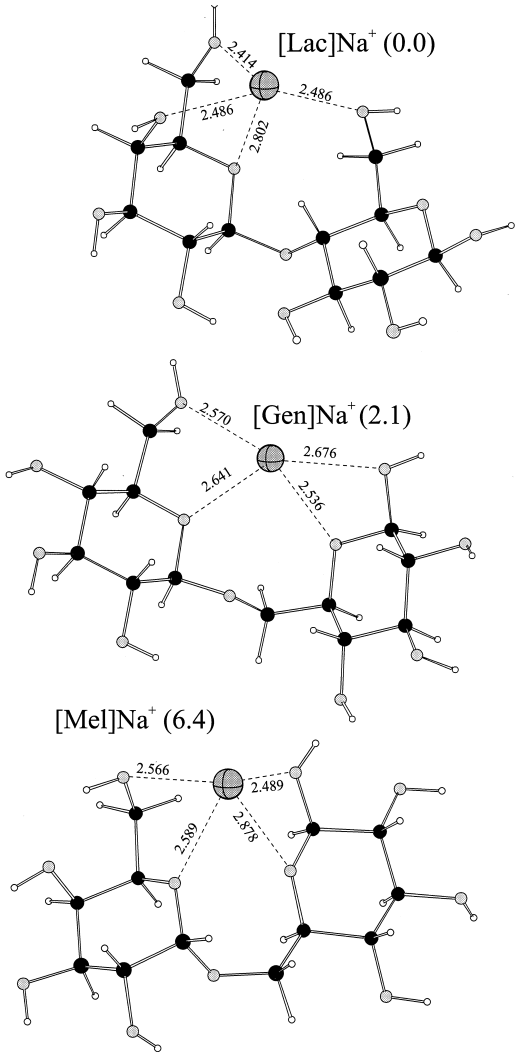

Fig. 8. Lowest energy conformers of the Na^+ complexes of disaccharides lactose, gentiobiose, and melibiose optimized by molecular mechanics using the MM2 force field. The numbers in parenthesis are relative steric energies in kilojoules per mole.

result of their overall larger sizes which affords them a higher polarizability and flexibility to interact with Na^+.

6. Conclusions

The Na^+ affinities determined in this study are consistent with the saccharides being multidentate ligands to Na^+. Each saccharide solvates the sodium ion differently, depending on the donor groups available. Compared to pentoses, hexoses form stronger Sac–Na^+ bonds because their hydroxymethyl substituent brings about a larger conformational flexibility and stronger inductive effects to sequester the approaching sodium cation. The involvement of the hydroxymethyl group in the binding of Na^+ is corroborated by the larger relative entropies of the hexoses vis à vis the pentoses. A further increase in both Na^+ affinity and entropy of Na^+ complexation is observed for the disaccharides which both carry a larger number of functional groups and more flexible rotors. The Na^+ affinities are found to be sensitive to changes in the saccharide stereochemistry. The $\Delta H^{o}_{Na^+}$ differences between specific stereoisomers are, however, quite small and necessitate an experimental method capable of probing small changes; this prerequisite is fortunately satisfied by the modified Cooks kinetic method used here, which can accurately measure small relative affinities and entropies.

Theoretical calculations of the Na^+ complexes indicate that the pyranose hemiacetal oxygen and the hydroxymethyl group (when available) participate in the binding of Na^+ and that the stereochemistry of the monosaccharide affects not only the number of ligands supplied to Na^+, but also the conformation adopted by the saccharide in order to optimally coordinate Na^+. The Na^+ affinities of isomeric saccharides and the computed relative energies of the corresponding [Sac]Na^+ follow the same order, pointing out that the Sac–Na^+ bond strengths primarily reflect the stability of the sodiated complexes.

The distinct Na^+ affinities of saccharide stereoisomers can be used for their structural differentiation. For this, it is not necessary to follow the rigorous approach outlined above. A simple series of MI or CAD spectra would be sufficient. Thus, an unknown Sac could be identified by pairing it with a given anchor, such as the dipeptide AA, and comparing the abundance ratio of [Sac]Na^+ to [AA]Na^+ to the ratios obtained from a series of known isomeric saccharides (calibrants) against the same anchor.

Acknowledgements

The authors thank Dr. Michael J. Polce for valuable suggestions and Dr. David S. Perry and Dr. David A. Modarelli for help with the theoretical calculations. They are grateful to the Ohio Board of Regents and the University of Akron for their financial support.

References

[1] K. Burger, Biocoordination Chemistry: Coordination Equilibria in Biological Active Systems, Ellis Horwood, New York, 1990.
[2] J.A. Cowan, Inorganic Biochemistry: An Introduction, VCH, New York, 1993.
[3] G. Puzo, J.-C. Prome, Org. Mass Spectrom. 19 (1984) 448.
[4] Y. Tondeur, A.J. Clifford, L.M. De Luca, Org. Mass Spectrom. 20 (1985) 157.
[5] G.E. Hofmeister, Z. Zhou, J.A. Leary, J. Am. Chem. Soc. 113 (1991) 5964.
[6] L.M. Teesch, J. Adams, Org. Mass Spectrom. 27 (1992) 931.
[7] M. Lipták, Z. Dinya, F.J. Sztaricskai, G. Litkei, J. Jekő, Org. Mass Spectrom. 27 (1992) 1271.
[8] J. Lemoine, B. Fournet, D. Despeyroux, K.R. Jennings, R. Rosenberg, E. de Hoffman, J. Am. Soc. Mass Spectrom. 4 (1993) 197.
[9] G.J.C. Paul, R. Théberge, M.J. Bertrand, R. Feng, M.D. Bailey, Org. Mass Spectrom. 28 (1993) 1329.
[10] L.C. Ngoka, J.-F. Gal, C.B. Lebrilla, Anal. Chem. 66 (1994) 692.
[11] K.P. Madhusudanan, T.S. Dhami, S. Katiyar, S.N. Suryawanshi, Org. Mass Spectrom. 29 (1994) 143.
[12] B. Domon, D.R. Mueller, W.J. Richter, Org. Mass Spectrom. 29 (1994) 713.
[13] D.J. Harvey, P.M. Rudd, R.H. Batemen, R.S. Bordoli, K. Howes, J.B. Hoyes, R.G. Vickers, Org. Mass Spectrom. 29 (1994) 753.
[14] B. Spengler, D. Kirsch, R. Kaufmann, J. Lemoine, Org. Mass Spectrom. 29 (1994) 782.
[15] M.H. Florencio, D. Despeyroux, K.R. Jennings, Org. Mass Spectrom. 29 (1994) 483.

[16] V. Kovácic, J. Hirsch, P. Kovác, W. Heerma, J. Thomas-Oates, J. Haverkanp, J. Mass Spectrom. 30 (1995) 949.
[17] M.T. Cancilla, S.G. Penn, J.A. Carroll, C.B. Lebrilla, J. Am. Chem. Soc. 118 (1996) 6736.
[18] M.R. Asam, G.L. Glish, J. Am. Soc. Mass Spectrom. 8 (1997) 987.
[19] K.L. Busch, G.L. Glish, S.A. McLuckey, Mass Spectrometry/Mass Spectrometry, VCH Publishers, New York, 1988.
[20] Applications of Mass Spectrometry to Organic Stereochemistry, J.S. Splitter, F. Turecek (Eds.), VCH, New York, 1994.
[21] (a)H. Suming, C. Yaozu, J. Longfei, X. Shuman, Org. Mass Spectrom. 20 (1985) 719; [21] (b) Y.-P. Tu, Y.-Z. Chen, S.-N. Chen, M.-L. Wang, Z.-Z. Jing, Org. Mass Spectrom. 25 (1990) 9.
[22] M. Sawada, L. Ouyang, Y. Takai, H. Yamada, T. Hanafusa, T. Kinoshita, T. Mochizuki, Chem. Lett. (1990) 1361.
[23] M. Sawada, M. Shizuma, Y. Takai, H. Yamada, T. Kaneda, T. Hanafusa, J. Am. Chem. Soc. 114 (1992) 4405.
[24] M. Sawada, Y. Okumura, M. Shizuma, Y. Takai, Y. Hidaka, H. Yamada, T. Tanaka, T. Kaneda, K. Hirose, S. Misumi, S. Takahashi, J. Am. Chem. Soc. 115 (1993) 7381.
[25] A. Fura, J.A. Leary, Anal. Chem. 65 (1993) 2805.
[26] A.P. New, N.J. Haskins, D.E. Games, Rapid Commun. Mass Spectrom. 7 (1993) 1099.
[27] M. Lipták, W. Heerma, Rapid Commun. Mass Spectrom. 7 (1993) 676.
[28] T.T. Dang, S.F. Pedersen, J.A. Leary, J. Am. Soc. Mass Spectrom. 5 (1994) 452.
[29] M. Coppola, D. Favretto, P. Traldi, G. Resnati, Org. Mass Spectrom. 29 (1994) 553.
[30] G. Smith, J.A. Leary, J. Am. Chem. Soc. 118 (1996) 3293.
[31] C. Guenat, R. Houriet, D. Stahl, J. Winkler, Helv. Chim. Acta 68 (1985) 1647.
[32] G. Hofmeister, J.A. Leary, Org. Mass Spectrom. 26 (1991) 811.
[33] T.K. Majumdar, F. Clairet, J.-C. Tabet, R.G. Cooks, J. Am. Chem. Soc. 114 (1992) 2897.
[34] R.G. Cooks, J.S. Patrick, T. Kotiaho, S.A. McLuckey, Mass Spectrom. Rev. 13 (1994) 287.
[35] C. Denekamp, A. Etinger, R.H. Fokkens, N. Khaselev, A. Mandelbaum, N.M.M. Nibbering, J. Mass Spectrom. 30 (1995) 1174.
[36] T. Vaisar, J. Urban, H. Nakanishi, J. Mass Spectrom. 31 (1996) 937.
[37] K. Vékey, G. Czira, Anal. Chem. 69 (1997) 1700.
[38] G. Puzo, J.-J. Fournie, J.-C. Prome, Anal. Chem. 57 (1985) 892.
[39] M. Sawada, L. Ouyang, Y. Takai, H. Yamada, T. Hanafusa, Chem. Lett. (1989) 1743.
[40] S.A. McLuckey, D. Cameron, R.G. Cooks, J. Am. Chem. Soc. 103 (1981) 1313.
[41] B.A. Cerda, C. Wesdemiotis, J. Am. Chem. Soc. 117 (1995) 9734.
[42] B.A. Cerda, C. Wesdemiotis, J. Am. Chem. Soc. 118 (1996) 11884.
[43] B.A. Cerda, C. Wesdemiotis, J. Am. Chem. Soc. 120 (1998) 2437.
[44] M.B. More, D. Ray, P.B. Armentrout, J. Phys. Chem. A 101 (1997) 831.
[45] X. Cheng, Z. Wu, C. Fenselau, J. Am. Chem. Soc. 115 (1993) 4844.
[46] Z. Wu, C. Fenselau, Rapid Commun. Mass Spectrom. 8 (1994) 777.
[47] M.J. Nold, B.A. Cerda, C. Wesdemiotis, J. Am. Soc. Mass Spectrom. 10 (1999) 1.
[48] K. Vékey, J. Mass Spectrom. 31 (1996) 445.
[49] S.L. Craig, M. Zhong, B. Choo, J.I. Brauman, J. Phys. Chem. 101 (1997) 19.
[50] M.J. Polce, M.M. Cordero, C. Wesdemiotis, P.A. Bott, Int. J. Mass Spectrom. Ion Processes 113 (1992) 35.
[51] (a) R.G. Cooks, J.H. Beynon, R.D. Caprioli, G.R. Lester, Metastable Ions, Elsevier, Amsterdam, 1973; (b) J.L. Holmes, Org. Mass Spectrom. 20 (1985) 169.
[52] M.J. Frisch, G.W. Trucks, H.B. Schlegel, P.M.W. Gill, B.G. Johnson, M.A. Robb, J.R. Cheesemann, T.A. Keith, G.A. Peterson, J.A. Montgomery, K. Raghavachari, M.A. Al-Laham, V.G. Zakrewski, J.V. Ortiz, J.B. Foresman, J. Cioslowski, B.B. Stefanov, A. Nanayakkara, M. Challocombe, C.Y. Peng, P.Y. Ayala, W. Chen, M.W. Wong, J.L. Andres, E.S. Replogle, R. Gomperts, R.L. Martin, D.J. Fox, J.S. Binkley, D.J. Defrees, J. Baker, J.J.P. Stewart, M. Head-Gordon, C. Gonzales, J.A. Pople, Gaussian 94, Revision B. 1, Gaussian, Inc., Pittsburgh, PA, 1995.
[53] Gaussian, Inc., Pittsburgh, PA.
[54] CambridgeSoft Corporation, Cambridge, MA.
[55] The CS MOPAC and MM2 programs are included in the Chem-3D software package [54].
[56] (a) S.J. Angyal, Adv. Carbohydr. Chem. Biochem. 42 (1984) 15; (b) H.S. El Khadem, Carbohydrate Chemistry: Monosaccharides and Their Oligomers, Academic, San Diego, 1988.
[57] E. De Pauw, Meth. Enzymol. 193 (1990) 201.
[58] B.C. Guo, B.J. Conklin, A.W. Castleman Jr., J. Am. Chem. Soc. 111 (1989) 6506.
[59] S.E. Barrows, J.W. Storer, C.J. Cramer, A.D. French, D.G. Truhlar, J. Comput. Chem. 19 (1998) 1111.
[60] P.L. Polavarapu, C.S. Ewig, J. Comput. Chem. 13 (1992) 1255.
[61] K.A. Jebber, K. Zhang, C.J. Cassady, A. Chung-Phillps, J. Am. Chem. Soc. 118 (1996) 10515.
[62] J.W. Brown, B.D. Wladkowski, J. Am. Chem. Soc. 118 (1996) 1190.
[63] S. Ha, J. Gao, B. Tidor, J.W. Brady, M. Karplus, J. Am. Chem. Soc. 113 (1991) 1553.
[64] B.P. van Eijck, R.W.W. Hooft, J. Kroon, J. Phys. Chem. 97 (1993) 12093.
[65] C.J. Cramer, D.G. Truhlar, J. Am. Chem. Soc. 115 (1993) 5745.
[66] B.A. Cerda, C. Wesdemiotis, unpublished results.
[67] J. March, Advanced Organic Chemistry: Reactions, Mechanisms, and Structure, 2nd ed., McGraw-Hill, Tokyo, 1977, p. 128.